Est. 1984

ORIENTAL JOURNAL OF CHEMISTRY
An International Open Access, Peer Reviewed Research Journal

www.orientjchem.org

ISSN: 0970-020 X
CODEN: OJCHEG
2023, Vol. 39, No.(5):
Pg. 1184-1193

Tunable Paramagnetism in Mn co-doped N: CdS Composite Nanoparticles

SURYA SEKHAR REDDY M[1] and KISHORE KUMAR Y B[2]*

[1]Department of Physics, JNTUA, Ananthapuramu, A.P, India.
[2]Department of Physics, SVCR Government Degree College, Palamaner, A.P, India.
*Corresponding author E-mail: msrphd2022@gmail.com

http://dx.doi.org/10.13005/ojc/390511

(Received: July 12, 2023; Accepted: September 21, 2023)

ABSTRACT

Manganese-co-doped N:CdS composite nanoparticles (CNps) have been prepared by using the co-precipitation method. 2-Mercaptoethonal is used as a surfactant to control the size of nanoparticles. X-ray diffraction (XRD) studies confirm the size of the particles in the nanorange. The Rietveld refinement with X'-pert high-score software studies show multiphase existence in as-prepared composite nanoparticles. The energy dispersive analyses of X-ray studies (EDAX) confirm the presence of doped Mn and nitrogen elements in CdS. The Fourier transform infrared spectroscopy (FTIR) studies confirm the presence of surfactant. The ultraviolet-visible spectroscopy studies (UV-Vis) show a clear blue shift in the band gap, which is an indication of the quantum confinement effect. The photoluminescence studies (PL) attribute the emission of a characteristically strong peak at λ = 632 nm, corresponding to the ($^4T_1 \rightarrow {}^6A_1$) transition, to the inclusion of Mn^{2+} in the core of the CdS lattice. The electron paramagnetic spectroscopy (EPR) studies show paramagnetic behavior. The hyperfine splitting constant (A) values around 7 mT from EPR confirms the inclusion of Mn^{2+} and N^{3-} in the tetrahedral sites of the CdS core. The variation in optical and magnetic properties of as-prepared composite nanoparticles has the potential for optoelectric and magnetoluminescence devices.

Keywords: Multiphase, Quantum confinement, Tetrahedral phase,

INTRODUCTION

Nanocrystalline CdS is well known as an easy-tunable, wide-direct-band gap semiconductor. It allows the doping of a wide variety of elements, ranging from s-block to f-block, as dopants. Depending on the nature of the dopant, many researchers reported modifications in structural, optical, electrical, and magnetic properties. Because of its easy-tunable properties, it is useful in materials science emerging to fabricate miniaturized smart devices[1].

Incorporation of a minute amount of transition metals (Ni, Co, Fe, Mn, Cr, Zn, etc.) into

the CdS lattice showed recognizable magnetic properties, hence, these materials are called diluted magnetic semiconductors[2,3] The CdS core is normally nonmagnetic; the transition metals are responsible for magnetic properties. In spite of all other transition metals, Mn has peculiar characteristics due to its half-field d-orbitals, which contribute to the formation of dimers with other dopant elements[1]. According to bound magnetic polaron theory (BMP), these dimers are responsible for the ferromagnetic and antiferromagnetic nature of DMS materials. The Mn has the ability to create additional traps inside the CdS core, which leads to modifications in luminescence properties. These compounds are called magnetoluminescence compounds[4].

In recent studies, the stability of DMS nanoparticles has been the main problem. The formation of secondary compounds increases stability[5-7]. Among all other eligible elements, nitrogen has the ability to exist in different ionic states (N^{3-}, N^{5-} and N^{3+}), suitable for either anionic or cationic replacement in CdS. The high electronegativity value allows it to form secondary compounds (dimers), and composites when co-doped with transition elements. The N^{3-}, which exists in a tetrahedral structure, is more stable than all other phases[8]. Mn^{2+} also exists in a tetrahedral phase when it is incorporated into CdS to form DMS, even though CdS changes its phase from cubic to hexagonal[1]. These properties of elements motivated the present study to prepare Mn-doped N:CdS, DMS nanoparticles using a surfactant-assisted simple co-precipitation method at room temperature and study their structural, optical, and magnetic properties.

Methodology

A simple surfactant-assisted chemical co-precipitation method was used to prepare composite nanoparticles. All chemicals used for synthesizing CdS, $Cd_{1-x}Mn_xN_{0.06}S_{0.94}$ (where x = 0, 0.02, 0.04, 0.06, and 0.0 8) CNps were Sigma Aldrich AR grade with 99.9% purity, hence no need of further purification. Cd $(CH_3COO)_2$ $2H_20$ (for cadmium) and $Mn(CH_3COO)_2$ $4H_2O$ (for manganese) were used as cationic precursors, while Na_2S (for sulfur) and thiourea (for nitrogen) were used as anionic precursors. 2-Mercaptoethanol was used as a capping agent. 0.2 M solutions of each compound were prepared using deionized water as a solvent, as per stoichiometry, and stirred for 30 minutes. The anionic precursor, sodium sulfide, was taken in a conical flask and placed on a magnetic stirrer. Another anionic precursor, thiourea, was added dropwise and stirred for 30 minutes. 0.5 mL of 2-mercaptoethanol (capping agent) was added dropwise and stirred for another 30 min to get a uniform solution. The cationic precursors were added simultaneously, dropwise with their stoichiometric ratio, and stirred for another 7 h to complete the reaction. The precipitates were filtered and washed several times with deionized water to remove impurities. The cleaned precipitates dried naturally for 48 h in the laboratory, and then they were ground into a fine powder.

As synthesized $Cd_{1-x}Mn_xN_{0.06}S_{0.94}$ (where x = 0, 0.02, 0.04, 0.06, and 0.08) and CdS CNps structural, elemental, morphological, optical, and magnetic properties were analyzed using the techniques shown in Table 1.

Table 1: List of techniques used for characterization of as-prepared CdS, $Cd_{1-x}Mn_xN_{0.06}S_{0.94}$ (where x = 0, 0.02, 0.04, 0.06, and 0.08) CNps

S. No	Characterization	Technique	Instrument/specification
1	Mineralogical	X-ray diffraction (XRD)	Bruker-D8 advance, Germany X-ray diffractometer with Cu-αK radiation wavelength-1.540Å
2	Phase analysis	Rietveld refinement	Simulation Software (X'pert high score)
3	Morphological	Field emission scanning electron microscope (FESEM)	Carl FESEM03-81
4	Elemental studies	EDAX	Oxford EDAX attached CarlFESEM
5	Bond energy	Fourier transform Infrared (FTIR) spectroscopy	Agilent cavy 360-FTIR,resolution=1 cm^{-1}
6	Optical	Ultraviolet, visible spectroscopy(UV-Vis)	Perkin-Elmer Lambda 950, diffuse reflectance mode Photoluminescence (PL)spectroscopy JY Fluorolog-3-11 spectrometer (9.5G HZ excitation X-Band)
7	Magnetic	Electron paramagnetic resonance spectroscopy (EPR)	JEOL Model JES FA200

RESULTS AND DISCUSSION

Elemental studies

The EDAX analysis of CdS, $Cd_{1-x}Mn_xN_{0.06}S_{0.94}$ (where x = 0, 0.02, 0.04, 0.06, and 0.08) CNps is shown in Fig. 1. These profiles confirmed the presence of doped elements (nitrogen and manganese) with their atomic concentrations in the as-prepared CNps shown in Table 2.

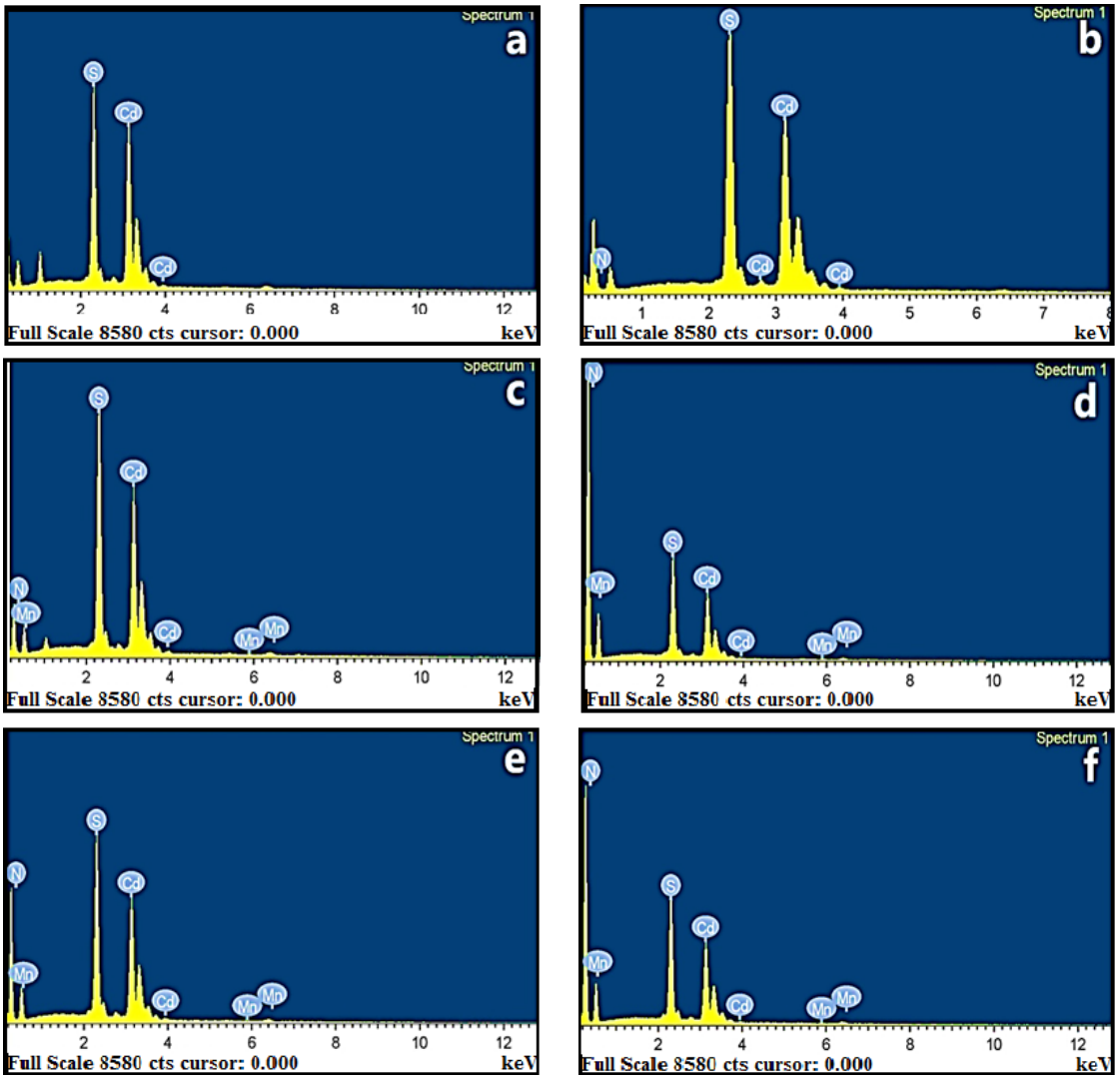

Fig. 1(a-f). The EDAX images of CdS, $Cd_{1-x}Mn_xN_{0.06}S_{0.94}$ (where x = 0, 0.02, 0.04, 0.06, and 0.08) CNps

Table 2: From the EDAX, the % of atoms present in as-prepared CdS, $Cd_{1-x}Mn_xN_{0.06}S_{0.94}$ CNps

$Cd_{1-x}Mn_xN_{0.06}S_{0.94}$	Elemental composition (in at. %)			
	Cd	Mn	N	S
x = 0.00	49.66	0.00	6.25	44.09
x = 0.02	47.12	1.94	6.18	44.76
x = 0.04	45.84	3.98	6.10	44.08
x = 0.06	44.06	5.88	6.12	43.84
x = 0.08	41.84	8.12	5.96	44.08
CdS	49.93	0.00	0.00	50.07

Structural Analysis

As-prepared CdS, $Cd_{1-x}Mn_xN_{0.06}S_{0.94}$ (where x = 0, 0.02, 0.04, 0.06, and 0.08) composite nanoparticles were displayed in Fig. 2 together with Rietveld refinement XRD patterns generated by the X'pert high score software. The samples showed well-resolved broadened peaks, which revealed that the samples exist in the nanoscale regime. The diffraction peaks were evident in the reflections corresponding to the planes of (110), (111), and (331). These show

that all samples exist in the cubic phase and are matched with JCPDS card No. 04-006-3897. The peak maxima shifting towards a higher 2θ was an indication of decreasing particle size with an increase in dopant concentration and the inclusion of dopant ions[3]. The peak broadening indicates the formation of secondary phases. The MnS phase was detected at higher concentrations (0.04, 0.06, and 0.08). The planes (110) at 27.3° and (111) at 45.6° of MnS were perfectly matched with JCPDS card No.40-1288 and reported data[9]. This shows the composite nature of as-prepared nanoparticles.

The size of the crystallites was estimated using the Debye-Scherer formula[10]. The values are tabulated in Table 3. The strain values decreased with an increase in dopant concentration, indicating an increase in the stability of the as-prepared composite nanoparticles[11].

Table 3: Crystallite size and the lattice strain and band gap of CdS, $Cd_{1-x}Mn_xN_{0.06}S_{0.94}$ (where x = 0, 0.02, 0.04, 0.06, and 0.08) composite nanoparticles

Compound	From XRD Crystallite Size(nm)	Lattice Strain
CdS	1.08	0.1400
$CdN_{0.06}S_{0.94}$	1.57	0.0994
$Cd_{0.98}Mn_{0.02}N_{0.06}S_{0.94}$	1.81	0.0991
$Cd_{0.96}Mn_{0.04}N_{0.0}6S_{0.94}$	1.66	0.0874
$Cd_{0.94}Mn_{0.06}N_{0.06}S_{0.94}$	1.22	0.0849
$Cd_{0.92}Mn_{0.08}N_{0.06}S_{0.94}$	1.14	0.0797

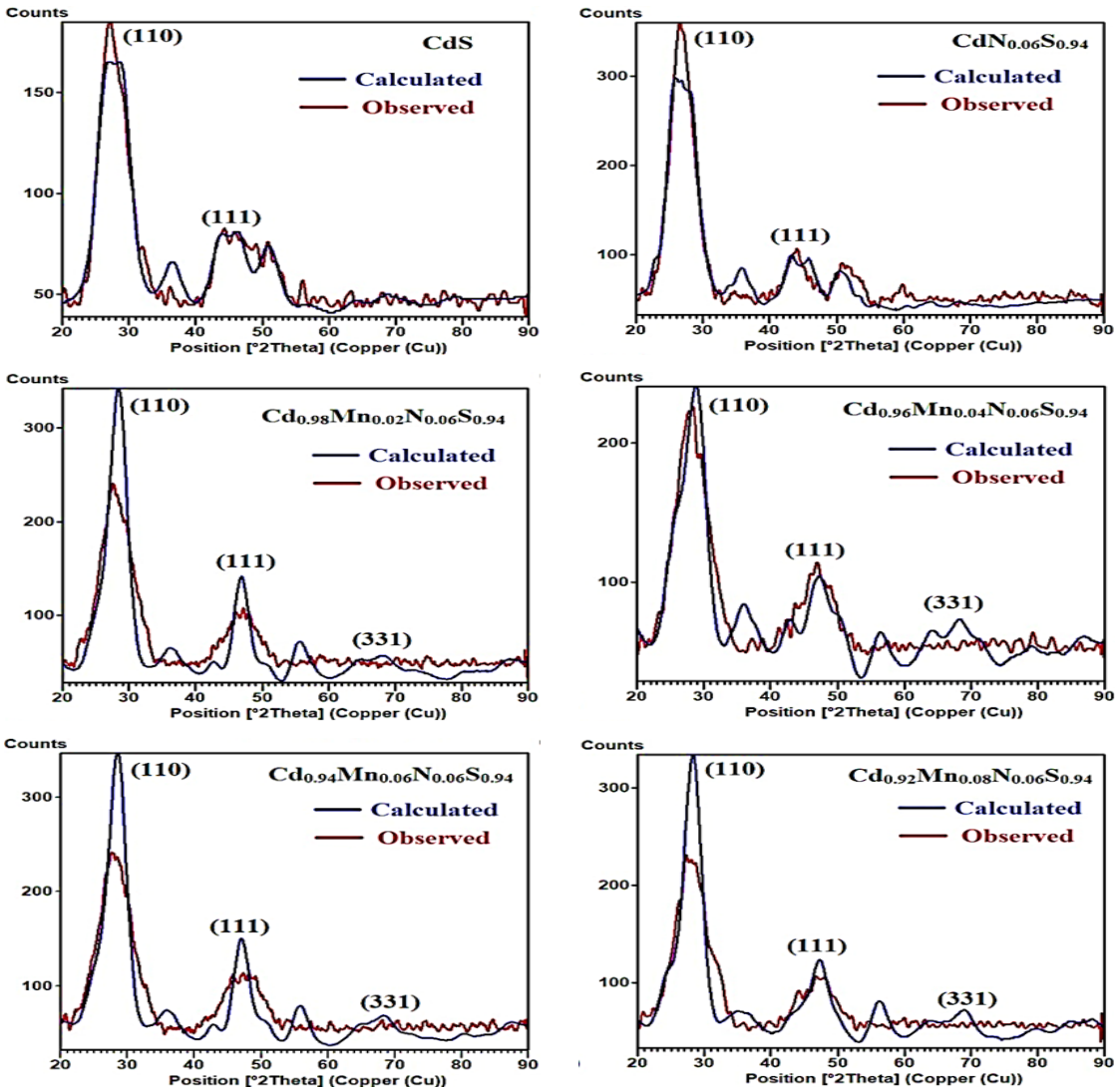

Fig. 2. Rietveld analysis of CdS, $Cd_{1-x}Co_xN_{0.06}S_{0.94}$ (where x = 0, 0.02, 0.04, 0.06, and 0.08), composite nanoparticles

Morphological studies

The FESEM images taken from the 100 nm distance of CdS, $Cd_{1-x}Mn_xN_{0.06}S_{0.94}$ (x = 0, 0.02, 0.04, 0.06, and 0.08) CNps, are shown in Fig. 3. The grains were densely packed. The size of the grains was not uniform and decreased with increasing concentration. This was observed due to grain boundary displacement[12]. The displacement leads to an increase in lattice strain and a modification of lattice parameters. The observed grain sizes of doped CNps were smaller than those of CdS nanoparticles.

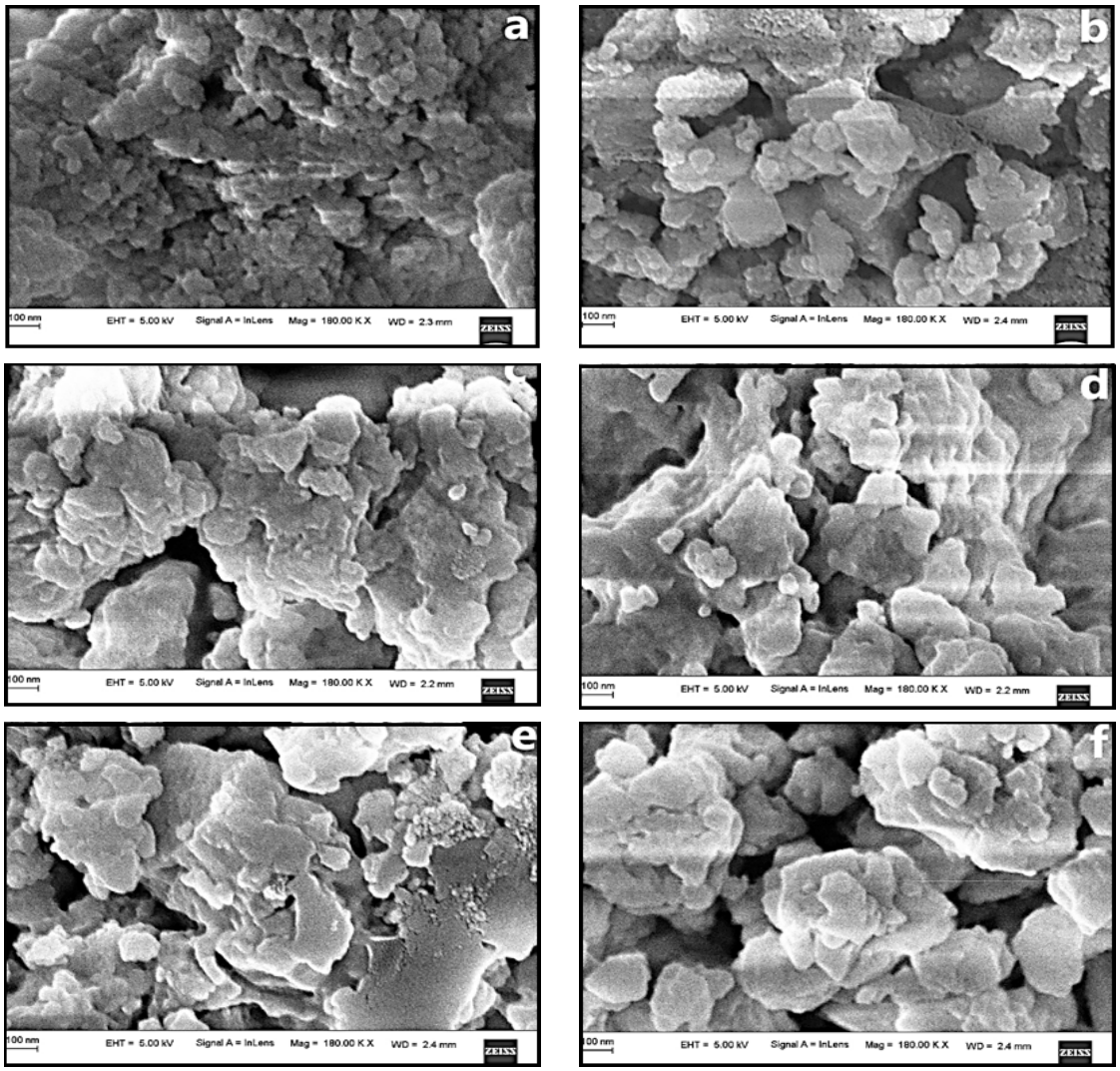

Fig. 3(a)–(f). FESEM images of CdS, $Cd_{1-x}Mn_xN_{0.06}S_{0.94}$ (where x = 0, 0.02, 0.04, 0.06, and 0.08) CNPs

Optical Studies

FTIR studies

Room-temperature FTIR spectra of as-prepared nanoparticles in the range 400-4000 cm^{-1} were shown in Fig. 4. The samples have the vibration bands of both surfactant and precursor components. The stretches below 800 cm^{-1} are ascribed to Cd, Mn, and S interactions, and the range from 800-4000 cm^{-1} represents organic functional groups. The vibration frequency observed between 500 and 650 cm^{-1} was attributed to the Mn-S bond[13]. In Mn:CdS, the frequency was observed at 640 cm^{-1} [14] but in this case, it was observed at 653 cm^{-1}. This stretch was not observed in pure Cd-S, which is present in all other as-prepared nanoparticles. The blue shift was attributed to nitrogen, which increases the force constant of

the bond. The stretches between 800 and 4000 cm^{-1} indicate the different functional groups mentioned in Table 4, which were present in all samples attributed to 2-mercaptoethanol[15]. The room-temperature FTIR analysis revealed the presence of Mn, nitrogen, and 2-mercaptoethonal, which was used as a surfactant to control the size of the as-prepared composite nanoparticles.

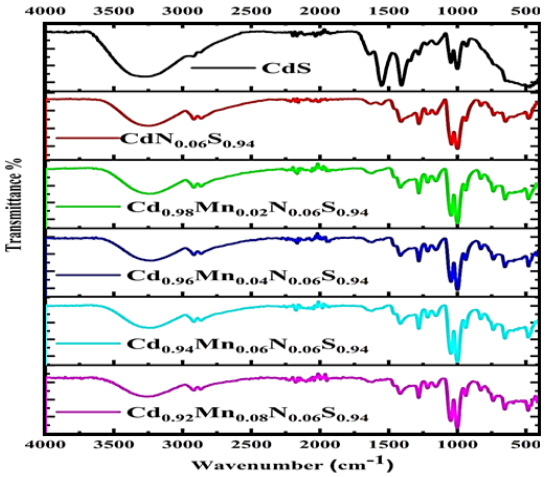

Fig. 4. FTIR spectra of CdS, $Cd_{1-x}Mn_xN_{0.06}S_{0.94}$ (where x = 0, 0.02, 0.04, 0.06, and 0.08) CNps

Table 4: FTIR stretching of CdS, $Cd_{1-x}Mn_xN_{0.06}S_{0.94}$ (where x = 0, 0.02,0.04, 0.06, and 0.08) CNps

S. No.	Wave number (cm^{-1})	Functional Group/Bond
1	478	Cd–S[16]
2	653.73	Cd-S
3	829.07	O-H
4	999.12	C-C
5	1046.25	C-N
6	1154.77	C-S
7	1217.04	$-CH_2$
8	1415.02	C=C
9	1625.53	H–O-H
10	1551.41	C=O
11	2918.19	$-CH_2$
12	3245.83	O-H

UV-Vis spectra

The UV-Vis spectra of CdS, $Cd_{1-x}Mn_xN_{0.06}S_{0.94}$ (where x = 0, 0.02, 0.04, 0.06, and 0.08) composite nanoparticles recorded in reflection mode are shown in Fig. 5a. The absorption band edge position of as-prepared composite nanoparticles was observed between 545 nm and 470 nm. For CdS, it was at 545 nm and then shifted to 470 nm. The clear blue shift in absorption band edges was indicating the widening of the band gap by the inclusion of nitrogen and Mn^{2+} in the CdS matrix. This is an indication of the quantum confinement effect[17].

In order to estimate the band gap values of as-prepared CdS, $Cd_{1-x}Mn_xN_{0.06}S_{0.94}$ (where x = 0, 0.02, 0.04, 0.06, and 0.08) composite nanoparticles, Tauc's plots were used. Taking the incident radiation energy 'hν' on the x-axis, $(\alpha h\nu)^2$ where 'ν' is the frequency of the incident light and 'α' is the absorption coefficient of the material on the y-axis, a plot was drawn. The extrapolation of the linear part of the graph to the x-axis gives the band gap value. The estimated band edge positions, band gap values are shown in Table 5. From the Table, the clear blue shift in band gap values confirms the quantum confinement effect due to the decrease in particle size in the nanoscale regime.

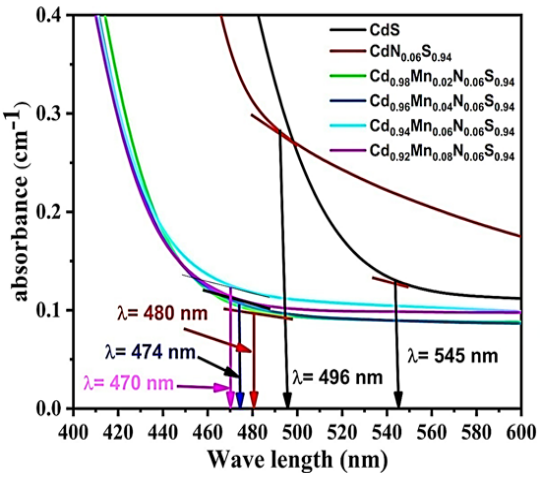

Fig. 5a. UV-Vis spectra absorption band edges of CdS, $Cd_{1-x}Mn_xN_{0.06}S_{0.94}$ (where x = 0, 0.02, 0.04, 0.06, and 0.08) CNps

Table 5: Band edge position, Band gap of CdS, $Cd_{1-x}Mn_xN_{0.06}S_{0.94}$ (where x = 0, 0.02, 0.04, 0.06, and 0.08) CNps

Compound	Band Edge Position(nm)	Band gap(eV)
CdS	545	2.54
$CdN_{0.06}S_{0.94}$	496	2.65
$Cd_{0.98}Mn_{0.02}N_{0.06}S_{0.94}$	480	4.43
$Cd_{0.96}Mn_{0.04}N_{0.06}S_{0.94}$	480	4.41
$Cd_{0.94}Mn_{0.06}N_{0.06}S_{0.94}$	474	4.44
$Cd_{0.92}Mn_{0.08}N_{0.06}S_{0.94}$	470	4.50

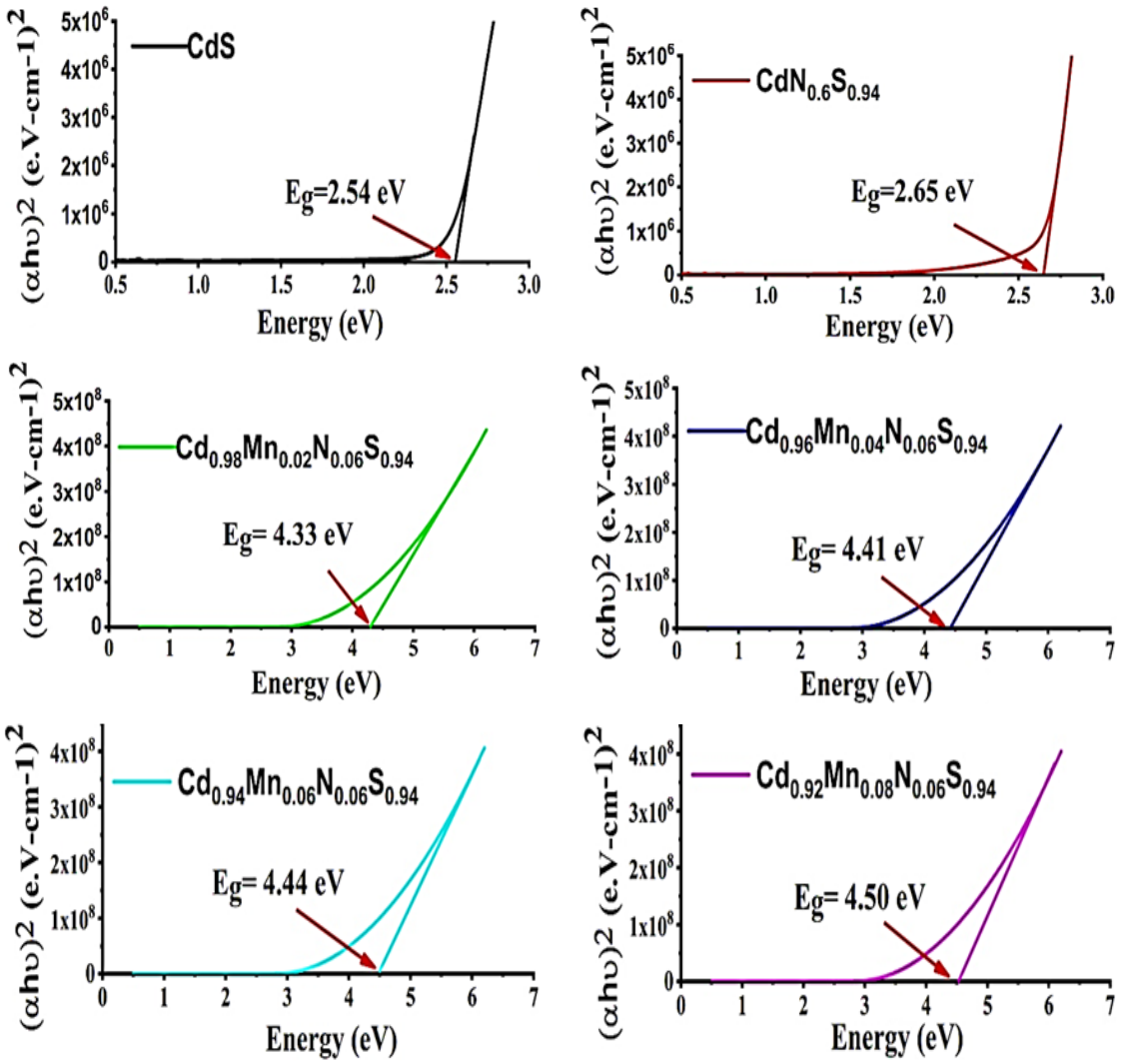

Fig. 5b. Tauc's plots of CdS, $Cd_{1-x}Mn_xN_{0.06}S_{0.94}$ (where x = 0, 0.02, 0.04, 0.06, and 0.08) CNps

PL studies

PL studies at room temperature were carried out to study the surface quality, defect levels, and interfaces of as-prepared nitrogen and Mn-doped CdS composite nanoparticles. Fig. 5c shows the PL spectra recorded at room temperature of CdS, $Cd_{1-x}Mn_xN_{0.06}S_{0.94}$ (where x = 0.02, 0.04, 0.06, and 0.08) composite nanoparticles with an excitation wavelength of 390 nm. The weak emission peaks were observed in all samples at 438 nm, 451 nm, and 467 nm, with variations in intensity[3]. These peaks originated due to the occupation of Mn^{2+} ions in the bottom level of the valency band. The lower intensity of the peak revealed the trapping of ions in interstitial vacancies. The strongest emission band, ranging from 550 nm to 750 nm, with a 632 nm emission-centred peak, was observed in all samples. The full width half maxima (FWHM) value of emission peaks decreased with increasing concentration, as was noticed. This indicates the broadening of peaks with dopant concentration. The intensity was maximum for $Cd_{1-x}Mn_xN_{0.06}S_{0.94}$ (x = 0.02), with further increases in Mn^{2+} concentration, the intensity decreased. The samples $Cd_{1-x}Mn_xN_{0.06}S_{0.94}$ (x = 0.06, 0.08) showed a quenching effect[15].

Mn^{2+} was responsible for luminescence intensity by encouraging radiative recombination of electrons and holes. The dopant induced quenching effect was common in nanoparticles due to the nonradiative recombination of many electrons and holes at higher concentrations. The

peak broadening was due to the trapping of Mn^{2+} ions in interstitial vacancies within the bands. The characteristic emission at the 632 nm peak is attributable to the transition between $^4T_1$ and $^6A_1$ of Mn^{2+} ion energy states. Neto *et al.,*[18] in their studies explained this characteristic emission was observed when Mn^{2+} ion substitutionally included within the CdS core. The slight red shift in characteristic emission peak was ascribed to narrowing of band gap[18] by inclusion of N, co-doped in CdS. The Murali *et al.,*[19] reported the absence of this yellow peak and photoluminescence peak present at 700 nm responsible for inclusion of Mn^{2+} at the surface of Mn doped CdS nanorods. Giribabu *et al.,*[20] reported the luminescence peak at 585 nm responsible for inclusion of Mn^{2+} at the surface of the CdS nanoparticles. The present photoluminescence study attributed to the inclusion of Mn^{2+} ion within the core of CdS nanoparticles. The lowering of intensity with increasing dopant concentration indicates non availability of free ions. This was attributed to the formation of anti-ferromagnetic secondary compounds (MnS)[21], found in XRD analysis. This confirms the composite nature of as-prepared composite nanoparticles.

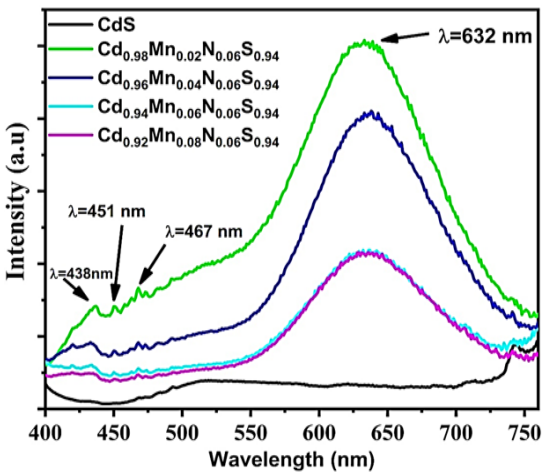

Fig. 5c. PL of CdS, $Cd_{1-x}Mn_xN_{0.06}S_{0.94}$ (where x = 0.02, 0.04, 0.06, and 0.08) CNps

Magnetic studies

EPR studies

In order to study the dopant ions oxidation states, the occupancy positions, phase, and magnetic properties of the present EPR studies were carried out. The EPR spectra of as-prepared CdS, $Cd_{1-x}Mn_xN_{0.06}S_{0.94}$ (where x = 0, 0.02, 0.04, 0.06, and 0.08) CNps, are shown in Fig. 6. In CdS, no EPR signals were found, which means no paramagnetic components exist in pure CdS. In nitrogen-doped samples, the stretched signal with 'g' slightly shifted from 2.181 to 2.214 was observed. In general, the EPR spectra of nitrogen (I = 1) show a triplet signal with an intrinsic 'g' value of 1.995, present study, no splitting of the EPR signal was found. This is due to an increase in the number of randomly distributed defects, an increase in the lifetime, and an increase in the interaction between the dopant ions. No reports are available for comparison.

The Mn^{2+} with electron spin (S=5/2) and nuclear spin (I=5/2) doped samples showed well separated sextant hyperfine splitting EPR components. The average hyperfine splitting constant (A) values were around 7 mT, and 'g' value was around 1.995. The characteristic 'g' value for Mn^{2+} is 2.0[22], and for nitrogen it is 1.995. Hence, the EPR signals present in the present study reveal the presence of nitrogen and Mn^{2+} in the as-prepared nanoparticles. Giribabu *et al.,*[20] reported the inclusion of the Mn^{2+} ion on the surface of the CdS Nps, with A = 95 G (9.5 mT), while Nag *et al.,* 2008[8] reported the substitutional inclusion of tetrahedral Mn^{2+} in the core of the CdS Nps, with A = 69 G (6.9 mT). In general, tetrahedral geometry phases possess lower energy and more stability[23].

Hence the 'A' value around 7 mT and flattened hyperfine peaks were indications of substitutional inclusion of the tetrahedral coordination Mn^{2+} ion in place of the Cd^{2+} ion. These results support the PL studies. In general, the tetrahedral phase is a more stable state compared to all other possible phases. The substitutional solvability of tetrahedral N^{3-} and Mn^{2+} ions in CdS increases the stability of CdS.

The zero-emission magnetic field (B_0), the width of the EPR signal (ΔB), spectroscopic 'g' factor, hyperfine splitting constant (A), and peak to peak intensity (I) of all samples were shown in Table 6. From the table, the number of spins (N_s) available was estimated using the formula $N_s = 0.285\ I\ (\Delta B)^2$, where 'I' is the peak-to-peak intensity of the EPR signal (a.u.) and 'ΔB' is the peak width (G). The obtained values of all prepared samples are shown in Table 6. From Table 6, the A, B_0, and 'g' values are almost independent of the doping concentration of Mn^{2+}. The intensity of the EPR signal increases with increases in doping concentration because of an increase in the number of spins attribute to the variation of room temperature paramagnetic property of as-prepared CNPs.

Table 6: B, g, A, I, and N_s values of CdS,$Cd_{1-x}Mn_xN_{0.06}S_{0.94}$ composite nanoparticles

Sample↓ property	B_0(mT)	ΔB (mT)	g	A (mT)	I (a.u)	No of spins(N_s)
x =0	309.00	296	2.214	---	375	
x=0.02	338.25	42	1.995	7.0	1720	86.5x106
x=0.04	338.00	42	1.995	7.0	2078	125x106
x=0.06	338.00	42	1.995	7.0	5083	293x106
x=0.08	338.00	42	1.995	7.0	5150	311x106
CdS	308.00	226	2.181	---	144	------

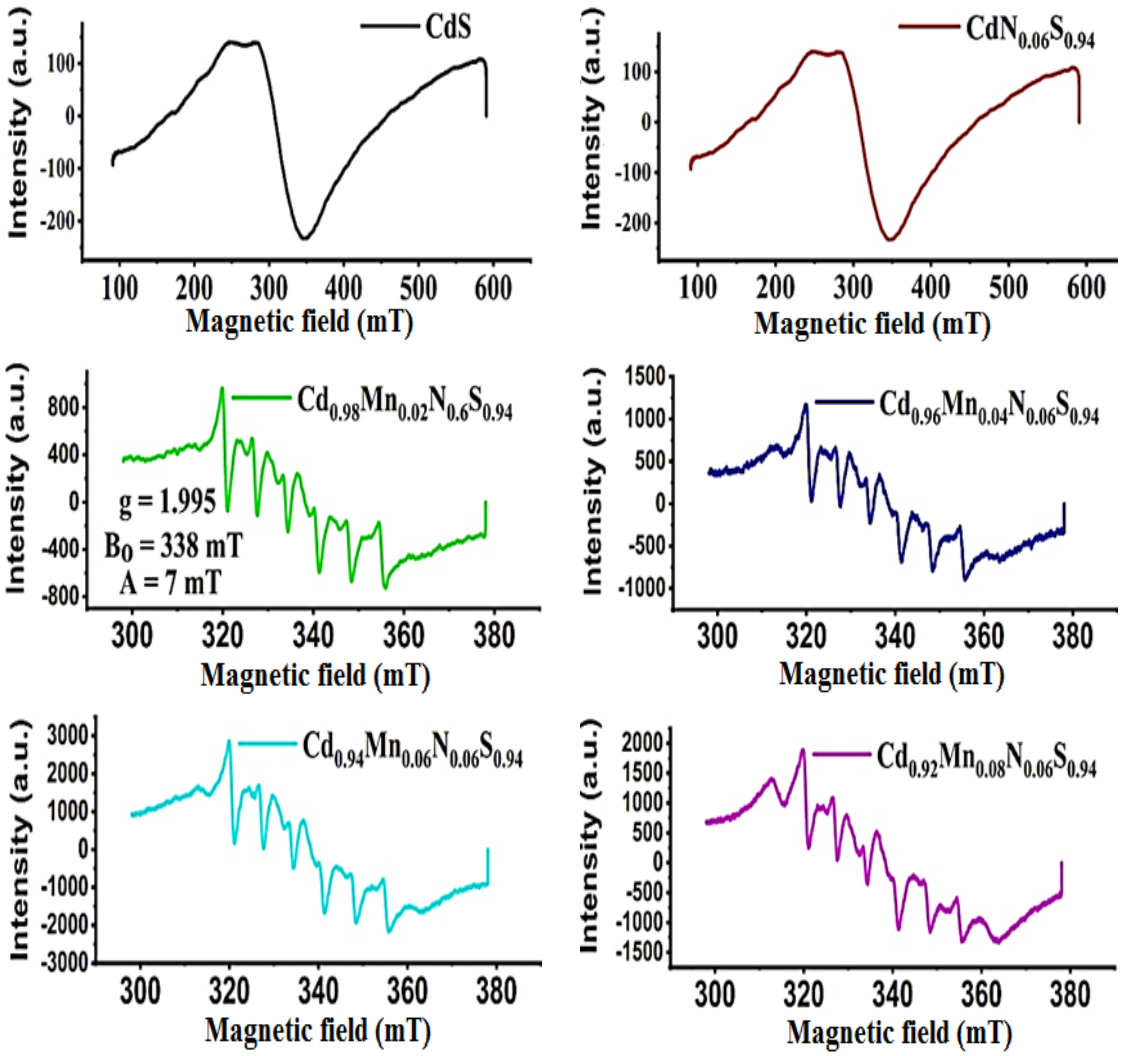

Fig. 6. EPR spectra of CdS, $Cd_{1-x}Mn_xN_{0.06}S_{0.94}$ (where x = 0, 0.02, 0.04, 0.06, and 0.08) CNps

CONCLUSION

In conclusion, manganese-co-doped N:CdS composite nanoparticles were successfully synthesized using the co-precipitation method. The addition of 2-mercaptoethonal as a surfactant effectively controlled the size of the nanoparticles. X-ray diffraction analysis confirmed that the particle size fell within the nano range. Rietveld refinement using X'-pert high score software revealed the composite nature of the as-prepared nanoparticles.

Energy dispersive analysis of X-rays (EDAX) confirmed the successful doping of manganese and nitrogen elements into the CdS lattice. Fourier

transform infrared spectroscopy (FTIR) studies provided further evidence of the presence of doped elements and the surfactant. Ultraviolet-visible spectroscopy (UV-Vis) demonstrated a clear blue shift in the band gap, indicating the occurrence of a quantum confinement effect.

Photoluminescence studies (PL) showed a distinctive peak at $\lambda = 632$ nm, corresponding to the ($^4T_1 \rightarrow {}^6A_1$) transition, which could be attributed to the incorporation of Mn^{2+} ions in the CdS lattice. Electron paramagnetic spectroscopy (EPR) analysis, along with a hyperfine splitting constant (A) values around 7 mT, confirmed the inclusion of Mn^{2+} and N^{3-} in the tetrahedral sites of the CdS core.

Overall, the successful synthesis of manganese-co-doped N:CdS nanoparticles, with controlled size, multiphase existence, and desirable optical and paramagnetic properties paves the way for their utilization in various technological fields requiring efficient optoelectronic and magneto-luminescent devises.

ACKNOWLEDGEMENT

We would like to express our sincere gratitude to the Sophisticated Analytical Instrumentation Facility (SAIF) at the Indian Institute of Technology (IIT) Chennai for their invaluable support and assistance in the characterization of our research samples.

Conflict of interest

The authors declare no conflicts of interest to disclose.

REFERENCES

1. Baruah, J. M.; Narayan, *J. Nonmagnetic Magn. Quantum Dots.*, **2018**, *87*, 78-93.
2. Ibraheem, Fatma.; Mahdy, Manal, A.; Mahmoud, Esmat, A.; Ortega, J.; Enrique Rogero, Celia.; Mahdy, Iman A.; El-Sayed, Afaf. *J. Alloys Compd.*, **2020**, *834*, 155-196.
3. Lin, C.Y.; Wang, W.H.; Lee, C.S.; Sun, K.W.; Suen, Y.W. *Appl. Phys. Lett.*, **2009**, *94*, 15.
4. Nag, A.; Sameer, S.; Gupta, S.S.; Prakash, A.; Ghangrekar, A.;Periasamy, N.; Sarma, D. D. *Bull. Mater. Sci.*, **2008**, *31*, 561–568.
5. Surya Sekhar Reddy, M.; Sai Vandana, C.; Kishore Kumar, Y. B. *J. Supercond. Nov. Magn.*, **2023**, *36*, 1243–1248.
6. Sain, S.; Kar, A.; Mukherjee, M.; Das, D.; Pradhan, S. K. *Adv. Powder Technol.*, **2016**, *27*, 1790–1799.
7. Yansong, Z.; Gang, C.; Yaoguang, Y.; Yujie, F.; Yi , Z,; Fang, H.; Zhonghui, H. *Phys. Chem. Chem. Phys.*, **2015**, *17*, 1870–1876.
8. Gadalla, A.; Almokhtar, M.; Abouelkhir, A.N. *Chalcogenide Lett.*, **2018**, *15*, 207–218.
9. Ma, Y.; Ma, Y.; Diemant, T.; Cao, K.; Kaiser, U.; Behm, R.J.; Varzi, A.; Passerini, S. *Chem Electro Chem.*, **2021**, *8*, 918– 927.
10. Salimian, S.; Farjami Shayesteh, S.; Salimian, S. *J. Supercond. Nov. Magn.*, **2012**, *25*, 2009–2014.
11. Nelli, D.; Roncaglia, C.; Minnai, C. *Adv. Phys. X.*, **2023**, *8*, 1.
12. Sharma, D.; Jha, R. *J. Alloys Compd.*, **2017**, *698*, 532–538.
13. Heiba, Z.K.; Mohamed, M.B.; Badawi, A.;Farag, N. M. *Chem. Phys. Lett.*, **2021**, *779*, 138877.
14. Giribabu, G.; Murali, G; Amaranatha Reddy, D.; Sambasivam, S.; Vijayalakshmi, R. P. *Mater. Lett.,* **2014**, *126*, 119-122.
15. Giribabu, G.; Murali, G; Amaranatha Reddy, D.; Liu C.; Vijayalakshmi, R.P.; *J. Alloys Compd.*, **2013**, *581*, 363–368.
16. Seoudi, R.; S. H. A. Allehyani, S. H. A.; Said, D. A.;Lashin A. R.; Abouelsayed, A.; *J. Electron. Mater.*, **2015**, *44*, 3367-3374.
17. Muruganandam S.; Anbalagan G.; Murugadoss G.;*Optik.*, **2017**, *131*, 826–837.
18. Neto E. S. F.; Dantas N.O.;Neto N. M. B.; Guedes I.; Chen F. *Nanotechnology.*, **2011**, *22*, 10.
19. Murali, G; Amaranatha Reddy, D.; Giribabu, G.; Vijayalakshmi, R.P.; Venugopal, R.; *J. Alloys Compd.*, **2013**, *581*, 849–855.
20. Giribabu, G.; Murali, G; Vijayalakshmi, R. P.; *Mater. Lett.*, **2014**, *117*, 298–301.
21. Masrour, R; Hlil, E. K.; Hamedoun, M.; Benyoussef, A.; Mounkachi, O.; *Chinese Phys.*B., **2012**, *21*, 8–12.
22. Amaranatha Reddy, D.; Sambasivam, S.; Murali, G; Poornaprakash, B.; Vijayalakshmi, R. P.; Aparna, Y.; Reddy, B. K.; Rao, J. L.; *J. Alloys Compd.*, **2012**, *537*, 208–215.
23. Kaur, M.; Kumar, V.; Singh, J.; Datt, J.; Sharma, R.; *Mater. Technol.*, **2022**, *37*, 2644–2658.